Available online at www.sciencedirect.com

ScienceDirect

www.elsevier.com/locate/jes

JES JOURNAL OF ENVIRONMENTAL SCIENCES

www.jesc.ac.cn

Efficient low-temperature soot combustion by bimetallic Ag–Cu/SBA-15 catalysts

Zhaojun Wen[1,**], *Xinping Duan*[1,**], *Menglin Hu*[1], *Yanning Cao*[2], *Linmin Ye*[1], *Lilong Jiang*[2,*], *Youzhu Yuan*[1,*]

1. *State Key Laboratory of Physical Chemistry of Solid Surfaces, National Engineering Laboratory for Green Chemical Productions of Alcohols-Ethers-Esters, College of Chemistry and Chemical Engineering, Xiamen University, Xiamen 361005, China*
2. *National Engineering Research Center of Chemical Fertilizer Catalyst, Fuzhou University, Fuzhou 350002, China*

ARTICLE INFO

Article history:
Received 6 September 2016
Revised 23 November 2016
Accepted 17 December 2016
Available online 14 February 2017

Keywords:
Silver
Copper
Bimetallic catalyst
Nanoalloy
Soot combustion
Thermal stability

ABSTRACT

In this study, the effects of copper (Cu) additive on the catalytic performance of Ag/SBA-15 in complete soot combustion were investigated. The soot combustion performance of bimetallic Ag–Cu/SBA-15 catalysts was higher than that of monometallic Ag and Cu catalysts. The optimum catalytic performance was acquired with the $5Ag_1$-$Cu_{0.1}$/SBA-15 catalyst, on which the soot combustion starts at T_{ig} = 225°C with a T_{50} = 285°C. The temperature for 50% of soot combustion was lower than that of conventional Ag-based catalysts to more than 50°C (Aneggi et al., 2009). Physicochemical characterizations of the catalysts indicated that addition of Cu into Ag could form smaller bimetallic Ag–Cu nanolloy particles, downsizing the mean particle size from 3.7 nm in monometallic catalyst to 2.6 nm in bimetallic Ag–Cu catalyst. Further experiments revealed that Ag and Cu species elicited synergistic effects, subsequently increasing the content of surface active oxygen species. As a result, the structure modifications of Ag by the addition of Cu strongly intensified the catalytic performance.

Introduction

Particulate matter (PM) mainly composed of soot and emitted by diesel engines can readily adsorb heavy metal species, organic matter, and other substances. Urban atmospheric PM that must be controlled primarily originates from soot particles and causes considerable atmospheric damage and health problems (Twigg, 2007). Therefore, the emission control of diesel soot has urgently become an important issue in environmental protection. As reported, PM can be efficiently and practically removed by using a diesel particulate filter (DPF) system (Bueno-López, 2014). PM can also be completely oxidized at considerable rates at 550–650°C. However, the exhaust temperatures of a DPF ranges from 300 to 400°C, which is too low to ignite soot combustion by oxygen molecules in the air, greatly causing DPF deactivated by the accumulation of soot particles (Sudarsanam et al., 2015). Importantly, other methods, including catalytic soot combustion, should be employed as potential alternatives to decrease oxidation temperatures. Numerous catalysts, including noble metals (Uchisawa et al., 1998), perovskite-type oxides (Ura et al., 2011), transition metals (Liang et al., 2008), earth alkali metals (Serra et al., 1997), and alkali metals (Aneggi et al., 2008), have also been conducted to reduce soot ignition temperature and to regenerate DPF completely at low temperatures.

* *Corresponding authors.*
** E-mail addresses: llj@fzu.edu.cn (Lilong Jiang), yzyuan@xmu.edu.cn (Youzhu Yuan).
These authors contributed equally to this work.

http://dx.doi.org/10.1016/j.jes.2016.12.021

Also, active oxygen species produced on the surface of catalysts and the interface between a metal phase and substrates have been improved due to substantial demands for highly catalytic soot combustion (Wei et al., 2011). Silver (Ag) is widely known as an efficient selective oxidation catalyst used in industrial processes (Aneggi et al., 2009) owing to its moderated activation of oxygen species and excellent selectivity in oxidation catalysis. Aneggi et al. (2009) reported the soot combustion activity of Ag-based catalysts deposited on Al_2O_3, CeO_2, and ZrO_2, suggesting that Ag enhances catalytic activity by promoting the adsorption–activation of oxygen molecules. Such enhancement can also be achieved by increasing the number of active oxygen species on the surface of catalysts (Corro et al., 2013; Wei et al., 2014). Unfortunately, the thermal stability of supported Ag-based catalysts is insufficient, especially at high temperatures or under reduction conditions. And these catalysts tender to deactivate severely through sintering attributed to their low-melting point (Kayama et al., 2010). As a practical protocol used to stabilize low-melting-point metals, high-melting-point metal additives function as highly thermal-stable bimetallic nanoalloy catalysts that can tune their catalytic performances.

On the other hand, due to their markedly different properties from monometallic catalysts, particularly in catalytic activities and stability, bimetallic catalysts coupled with ordered hexagonal mesoporous silica SBA-15 have been extensively investigated (Czaplinska et al., 2014; Liu et al., 2008). For instance, Au–Cu and Au–Ag nanoalloys exhibit a more efficient catalytic performance than that of monometallic counterparts in hydrogenation catalysis (Wang et al., 2012b; Zheng et al., 2013; Zhou et al., 2015b). Noble metal nanomaterials, such as Ag or Au nanoparticles (NPs), can be practically stabilized by formulating their nanoalloys with cost-effective metals, such as copper (Cu) or nickel (Ni) (Wang et al., 2012b; Zhou et al., 2015b). The geometric and electronic properties of nanoalloys can also be effectively tuned by controlling their composition and size; as a consequence, their catalytic performances can be influenced (Zheng et al., 2013; Wang et al., 2012b; Liu et al., 2008). In practical consideration, DPF is highly complicated because it involves complex reaction conditions. Thus, the substrate, such as SBA-15, should be selected on the basis of their optimum properties, including high thermal stability and efficiency in soot combustion exhaust environments. SBA-15 is characterized by thermal stability, high corrosion resistance, high surface area, and abundant diffusion channels (Zhao et al., 1998). Thus SBA-15-supported catalysts are considered to be capable of increasing the residence time and deposition rate of soot particles on the surface of catalysts, presenting a higher performance for the complete soot combustion.

In our study, SBA-15 supported Ag–Cu bimetallic catalysts (Ag–Cu/SBA-15) were prepared for the complete soot combustion. Our results revealed that the addition of a small amount of Cu to Ag nanomaterials promoted small particle formation, high dispersion, and excellent thermal stability under oxidation conditions. The Ag–Cu bimetallic catalysts could induce higher concentration of active oxygen species. The performance of the prepared catalysts in low-temperature soot combustion was more efficient than that of their monometallic counterparts.

1. Materials and methods

1.1. Catalyst preparation

Ordered mesoporous silica SBA-15 was synthesized in accordance with a previously described method (Zhao et al., 1998). Briefly, mesoporous SBA-15 was synthesized by using tetraethyl orthosilicate (TEOS) as a silica source and poly(ethylene oxide)-block-poly(propylene oxide)-block-poly(ethylene oxide) triblock copolymer (Aldrich, M_{av} = 5800, $EO_{20}PO_{70}EO_{20}$, P_{123}) as the structure-directing agent. In a typical synthesis, 6.0 g of P123 block copolymer was dissolved with stirring in a solution of 156 mL of water and 30 mL of HCl (4 M), and then 13.8 mL of TEOS was added with stirring at 308 K. After being stirred for 24 hr at 308 K, the gel solution was transferred into a Teflon bottle and heated at 370 K for 24 hr. Then the solid product calcined at 823 K for 6 hr to produce the final SBA-15 solid for the catalyst preparation. Bimetallic Ag–Cu/SBA-15 catalysts with a preset Ag loading of 5 wt.% were prepared with a co-impregnation method. In brief, quantitative amounts of $AgNO_3$ and $Cu(NO_3)_2{\cdot}3H_2O$ were dissolved in deionized water. SBA-15 was then added to the solution, and the resulting mixture was vigorously stirred and subjected to aging at room temperature for 12 hr overnight. The obtained powder was dried at 100°C overnight and calcined at 500°C for 4 hr to produce the final catalyst, which is denoted as $5Ag_1$-Cu_x/SBA-15, where x represents the atomic ratio of Cu and Ag. Monometallic Ag/SBA-15 and Cu/SBA-15 catalysts were also prepared using the same procedure.

1.2. Catalyst characterizations

The X-ray diffraction (XRD) patterns of the catalyst samples were obtained by using a PANalytical X'pert Pro diffractometer with Cu-K_α radiation (λ = 0.15418 nm) at a scanning angle (2θ) ranging from 10° to 90°. The tube voltage was 40 kV, and the current was 30 mA. Each XRD pattern was identified by matching the results with reference patterns included in the JCPDS database.

Transmission electron microscopy (TEM) images were obtained on a Tecnai F30 TEM operated at an acceleration voltage of 300 kV. The powdered catalyst was ultrasonically dispersed in ethanol at room temperature for 30 min. The as-obtained solution was then dropped into carbon-coated Cu grids. The statistical mean diameter of the NPs was measured by counting at least 200 particles for each catalyst from the TEM images.

The N_2 adsorption–desorption isotherms of catalysts were measured at −196°C by using a Micromeritics TriStar II 3020 porosimetry analyzer. The samples were degassed at 300°C for 3 hr prior to measurements. Specific surface area (S_{BET}) was calculated using the Brunauer–Emmett–Teller (BET) method, in which the isotherm data in a relative pressure (P/P_0) range of 0.05 to 0.30 were adopted. Total pore volume (V_{pore}) was derived from the absorbed N_2 volume at a relative pressure of approximately 0.99.

The ultraviolet–visible light (UV–Vis) diffuse reflectance spectra (DRS) of the as-reduced catalysts were obtained on a UV–Vis-Near infrared (NIR) Cary 5000 scanning spectrophotometer.

All catalyst precursors were freshly reduced in 5% H_2–95% N_2 atmosphere at 420°C for 3 hr. The as-reduced samples were carefully protected in a nitrogen atmosphere at room temperature before UV–Vis DRS measurements.

The metallic loadings of the samples were determined by inductively coupled plasma optical emission spectrometry (ICP–OES) using a Thermo Elemental IRIS Intrepid II XSP.

X-ray photoelectron spectroscopy (XPS) was conducted using a JPS-9010MC photoelectron spectrometer equipped with an Al–K_α X-ray radiation source ($h\nu$ = 1486.6 eV). Before measurements were performed, each sample was pressed into a thin disk and pretreated in an atmosphere of 5% H_2–95% N_2 at 420°C for 3 hr. The pretreated samples were also carefully collected in a nitrogen atmosphere before XPS measurements were carried out. The binding energy (BE) was calibrated using C 1s peak at 284.6 eV as a reference with an uncertainty of ±0.2 eV.

1.3. Catalytic soot combustion

The catalytic soot combustion activity of the catalysts was evaluated by the temperature-programmed oxidation (soot-TPO) technique using commercially available Printex-U soot (Degussa) as the model reactant. Typically, the soot was mixed with the catalyst in a weight ratio of 1:10 using a spatula for 5 min to obtain a loose contact. The soot/catalyst mixture was heated in a stream of 5% O_2 balanced with He at a constant rate of 10°C/min. To evaluate activity, we used the temperature at which 50% of weight loss is observed (T_{50}, corresponding to the temperature at which 50% of soot is converted under working conditions). The reproducibility of results was tested by running experiments on similar samples thrice, and T_{50} was consistently within ±5°C. The outcoming gases at various temperatures were analyzed by using a gas chromatograph in a TDX-01 capillary column with a thermal conductivity detector (TCD).

Activation energy was obtained *via* Ozawa method on the basis of DTA data (Ozawa, 1965). Each DTA pattern provides the temperature ($T_{\alpha,i}$) at which an "α" fixed fraction of carbon is burned during the DTA run and performed with the heating rate φ_i (φ_i = 5, 10, 15°C/min). Activation energy can be determined based on the fitted least square of the log(φi) *versus* T_α^{-1} data series by using the following equation:

$$\log(\varphi_i) = -0.4567\left(\frac{E_a}{RT_{\alpha,i}}\right) + B$$

where B is a constant whose value depends on the exponential factor in Arrhenius equation and on the fixed fraction of burned carbon at which $T_{\alpha,i}$ is calculated.

2. Results and discussion

2.1. Catalytic activity measurement

The catalytic performances of Ag–Cu/SBA-15 catalysts with varying Ag/Cu atomic ratios were initially examined in respect of soot combustion *versus* reaction temperature (Fig. 1). All of the samples exhibited a high specific surface area (Table 1 and Table S2). The high specific surface area and mesoporous structure of catalysts are considered to promote the contact between the soot particles and the active sites of the catalysts. These properties favor soot combustion implicated in diffusion and heat transport.

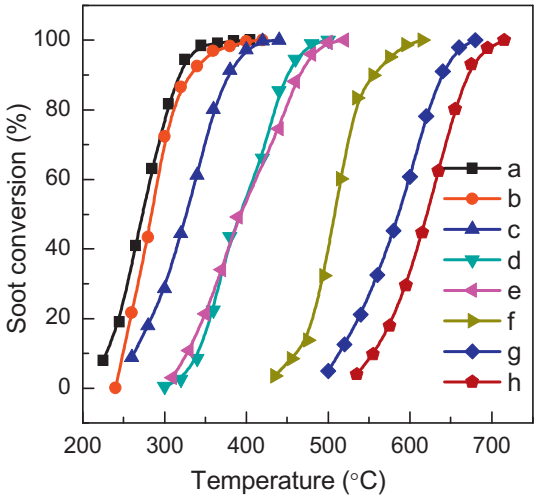

Fig. 1 – Soot conversion *versus* temperature of the monometallic and bimetallic catalysts. (a) 5Ag_1-$Cu_{0.1}$/SBA-15, (b) 5Ag_1-$Cu_{0.05}$/SBA-15, (c) 5Ag/SBA-15, (d) 5Ag_1-$Cu_{0.2}$/SBA-15, (e) 5Ag_1-$Cu_{0.4}$/SBA-15, (f) 5Cu/SBA-15, (g) SBA-15, and (h) pure soot.

The catalytic activities of the Ag–Cu bimetallic catalysts are shown in Fig. 1, and the corresponding results are summarized in Table 1. Soot combustion was catalyzed by all of the samples, even the respective blank SBA-15. This experiment verified the importance of the diffusion effect induced by mesoporous SBA-15. The blank SBA-15 substrate provided higher T_{ig}, T_{50}, and T_f of 500°C, 600°C, and 660°C, respectively. Bare soot was also used and automatically ignited with molecular oxygen. Thus, much higher T_{ig}, T_{50}, and T_f of 535°C, 655°C, and 695°C, respectively, were obtained. By contrast, the monometallic and bimetallic catalysts comprising Ag, Cu, or Ag–Cu significantly lowered the combustion temperatures, but the catalytic activities varied depending on the Ag/Cu atomic ratios. Among the bimetallic Ag–Cu bimetallic catalysts, the 5Ag_1-$Cu_{0.1}$/SBA-15 catalyst exhibited the highest catalytic activity with T_{ig}, T_{50}, and T_f of 225°C,

Table 1 – Surface area and catalytic performance of soot oxidation on Ag–Cu bimetallic catalysts with different atomic ratios.

Catalyst [a]	S_{BET} (m^2/g)	T_{ig} (°C) [b]	T_{50} (°C) [c]	T_f (°C) [d]
Pure soot	–	535	655	700
SBA-15	743	500	600	660
5Ag/SBA-15	492	270	360	495
5Cu/SBA-15	633	435	510	565
5Ag_1-$Cu_{0.05}$/SBA-15	445	240	300	420
5Ag_1-$Cu_{0.1}$/SBA-15	438	225	285	410
5Ag_1-$Cu_{0.2}$/SBA-15	430	300	460	520
5Ag_1-$Cu_{0.4}$/SBA-15	420	310	470	510

[a] Conditions: 5% O_2 and 95% He, 50 mL/min, the mass ratio (catalyst/soot) was set at 10:1.
[b] T_{ig}: starting temperature of soot ignition.
[c] T_{50}: the temperature that50% of soot is oxidized.
[d] T_f: finished temperature of soot combustion.

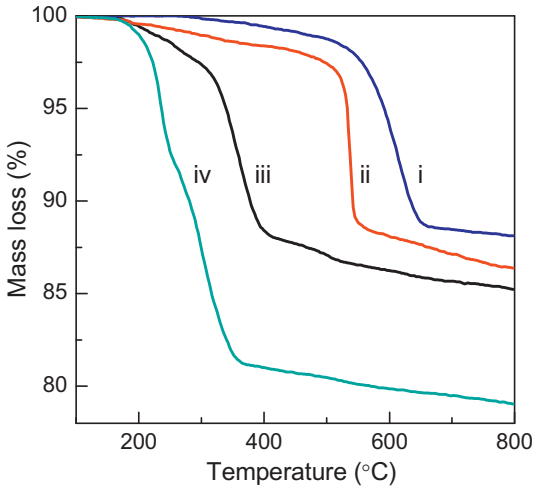

Fig. 2 – TG curves of the samples showing catalytic performances. (i) SBA-15, (ii) 5Cu/SBA-15, (iii) 5Ag/SBA-15, and (iv) $5Ag_1$-$Cu_{0.1}$/SBA-15. Reaction conditions: air flow rate = 50 mL · min^{-1}, mass ratio of catalyst/soot = 10:1.

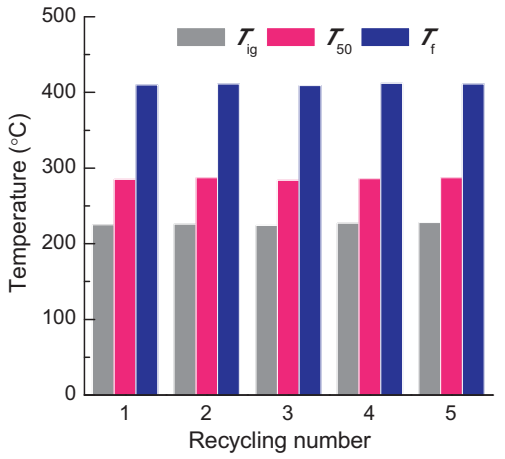

Fig. 3 – Catalytic soot combustion of $5Ag_1$-$Cu_{0.1}$/SBA-15 for five cyclic tests.

285°C, and 410°C, respectively. The catalytic activity increased as the Cu loading increased from 0.05% to 0.1%, but a higher Cu loading did not linearly improve the catalytic activity. This phenomenon is likely due to the overloading of Cu that blocks the active Ag sites on the surface. These results suggest that the catalytic properties of monometallic Ag catalyst are tuned by the introduction of low Cu concentration (Liu et al., 2008).

The representative catalysts were selected and evaluated in an air flow on a thermogravimetric (TG) analyzer (NETZSCH-TG209F3) (Fig. 2). The activities of these catalysts exhibited the following pattern: $5Ag_1$-$Cu_{0.1}$/SBA-15 >5Ag/SBA-15 > 5Cu/SBA-15 > SBA-15. The reactivity results of monometallic and bimetallic catalysts are consistent with those of soot-TPO evaluation (Fig. 2). The thermal stability of catalysts is recognized as an important parameter of the superior performance of catalysts. The thermal stability test results of 5Ag/SBA-15 and 5Cu/SBA-15 catalysts for soot combustion are listed in Table S1 (Supporting information). As indicated, the 5Ag/SBA-15 catalyst showed poor thermal stability for the soot combustion in three cyclic tests, whereas the Cu/SBA-15 catalyst presented a better thermal stability than Ag/SBA-15, although the initial reactivity of the former was inferior to the latter. The bimetallic $5Ag_1$-$Cu_{0.1}$/SBA-15 could maintain a high catalytic activity with negligible declining tendency in five cyclic tests (Fig. 3). Thus, the bimetallic catalysts composed of Ag and Cu, in addition to their enhanced activity, exhibited a high thermal stability for the soot combustion than that of their monometallic counterparts. The finding strongly verified our hypothesis and expectation. These results also reveal that the higher melting point of Cu species can likely stabilize Ag catalysts possessing low-melting points (Cao and Veser, 2009).

2.2. Catalyst characterization

The representative catalysts were selected to characterize and reveal the intrinsic correlation between catalytic performance and physicochemical properties and to gain insights into the promoting effects of Cu on the Ag catalyst in soot combustion. In addition to the characteristic lines belonging to SBA-15 support, the diffraction peaks of Ag or Cu NPs species were hardly detected by the powder XRD patterns of the samples (Fig. S1). In general, the introduction of Cu to the Ag/SBA-15 slightly changes the XRD patterns of the catalyst. Due to the detect limitation in XRD patterns when the particle size is smaller than 4 nm, we estimated the particle size variation of monometallic and bimetallic catalysts from the TEM images (Table S2). The TEM observation indicated that the monometallic and bimetallic nanomaterials were highly dispersed on the surface of the catalysts. The high-resolution TEM images of three typical monometallic and bimetallic catalysts, namely, Ag/SBA-15, Cu/SBA-15, and $5Ag_1$-$Cu_{0.1}$/SBA-15, are shown in Fig. 4. The SBA-15 substrate was well prepared with a clear mesoporous channel and thus provided high surface area and sufficient diffusion for small molecules (Fig. 4a). With respect to monometallic Ag and Cu catalysts (Fig. 4b and c), the TEM images showed similarities with highly dispersed Ag and Cu NPs, respectively. The $5Ag_1$-$Cu_{0.1}$/SBA-15 catalyst favored a more distinct dispersion of NPs with a smaller particle size of approximately 2.6 nm than Ag/SBA-15 catalyst with a particle size of 3.7 nm NPs (Fig. 4d, e, and f). The TEM results are consistent with the XRD patterns, indicating that the approach used to prepare bimetallic catalysts is valid. We also analyzed the HRTEM of bimetallic particles (inset in Fig. 4d), and the interval of lattice fringes was 0.239 nm corresponding to Ag (111) crystalline planes of cubic Ag (Zhou et al., 2015b) and revealing the morphological characteristics of bimetallic NPs following reduction.

As a powerful technique, UV–Vis is applied to examine the interaction among different metals and the formation of an alloy. Fig. 5 illustrates the variation of the UV–Vis spectra of Ag–Cu/SBA-15 with increasing Cu concentration compared with the corresponding monometallic Ag/SBA-15 and Cu/SBA-15 catalysts. For the small particles of most *d*-block metals, such as Cu, Ag, and Au, the absorption in the UV–Vis range is continuous across the range (Creighton and Eadon, 1991). The Ag/SBA-15 catalyst presented a sharp absorption peak at around 410 nm (Fig. 5), which typically reveals the well-known surface plasma resonance (SPR) band of dispersed Ag NPs. By

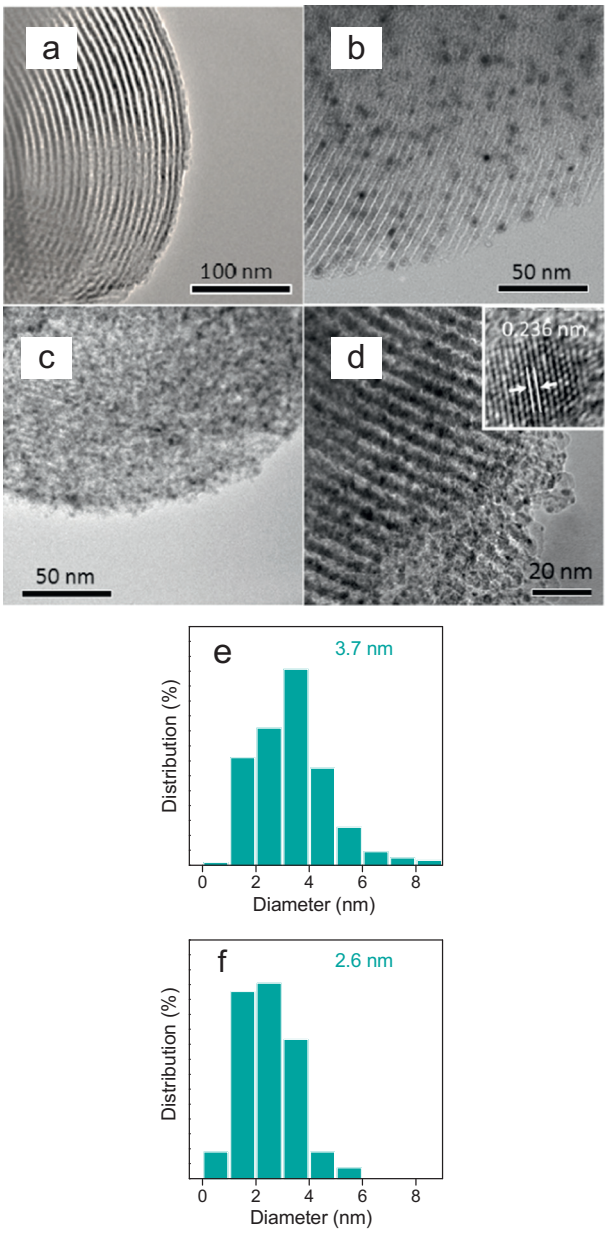

Fig. 4 – TEM images of as-prepared (a) SBA-15 support, (b) Ag/SBA-15, (c) Cu/SBA-15, and (d) $5Ag_1$-$Cu_{0.1}$/SBA-15. (e) and (f) are the particle size distributions of Ag/SBA-15 and $5Ag_1$-$Cu_{0.1}$/SBA-15, respectively, the inset image in (d) is the high-resolution TEM of separated NPs on $5Ag_1$-$Cu_{0.1}$/SBA-15 catalysts. TEM: transmission electron microscopy.

contrast, The Cu/SBA-15 catalyst provided a weak and broad SPR band at approximately 600 nm. For the Ag–Cu/SBA-15 catalysts with varying compositions by addition of Cu into Ag, the SPR band in the intermediate positions between those of the monometallic Ag and Cu counterparts could be observed. This finding indicates the physical mixture of the individual metals (Huang et al., 2013; Zhou et al., 2015b). As the Cu/Ag atomic ratio was increased, the SPR band gradually became red shifted corresponding to the formation of nanoalloy materials and the change in the electronic structure of bimetallic samples after Cu was introduced to the Ag base. These results suggest the formation of the Ag–Cu alloy. These findings are also consistent with our previously reported results on nanoalloy catalysts in hydrogenation (Zheng et al., 2013). Temperature-programmed reduction (TPR) and XPS profiles confirmed the chemical interaction, instead of a simple physical mixing between Ag and Cu species, resulting in the inhibition and shifting of the SPR band (Zhou et al., 2015b).

TPR characterization reveals the reducibility of metallic nanomaterials, as determined by the microstructure of metal species and relevant oxide support interaction (Xu et al., 2011; Zhou et al., 2015b). Fig. 6 displays the H_2–TPR profiles of SBA-15-supported Cu, Ag, and Ag–Cu catalyst precursors. The monometallic Cu/SBA-15 exhibited a reduction peak near 242°C, which was attributed to the reduction of highly dispersed Cu^{2+} or Cu^{+} to Cu^{0} and copper phyllosilicate to Cu^{+} (Chen et al., 2008). The other monometallic 5Ag/SBA-15 catalyst obtained one peak at around 131°C, which belonged to the reduction of Ag^{+} transforming into the metallic silver phase. However, the reduction peaks of the bimetallic samples gradually shifted to a lower temperature as the Cu/Ag atomic ratio increased because of Ag–Cu/SBA-15. The introduction of Cu likely decreased the reduction temperature and thus implied that significant interactions occurred between Ag and Cu species. The TPR results verified the UV–Vis SPR findings, which revealed that the bimetallic Ag–Cu nanoalloy was successfully synthesized.

XPS was further employed to explore the electronic structure and the surface valence state of monometallic or bimetallic nanomaterials. The Ag 3d XPS spectra of the as-reduced Ag/SBA-15 revealed two peaks at 367.6 and 373.6 eV (Fig. 7a), which was slightly lower than those of metallic Ag $3d_{5/2}$ and Ag $3d_{3/2}$. The results are consistent with our previous observation (367.9 to 368.1 eV and 373.9 eV to 374.1 eV, respectively) (Zhou et al., 2015b). These results are relevant to the interaction between Ag species with support

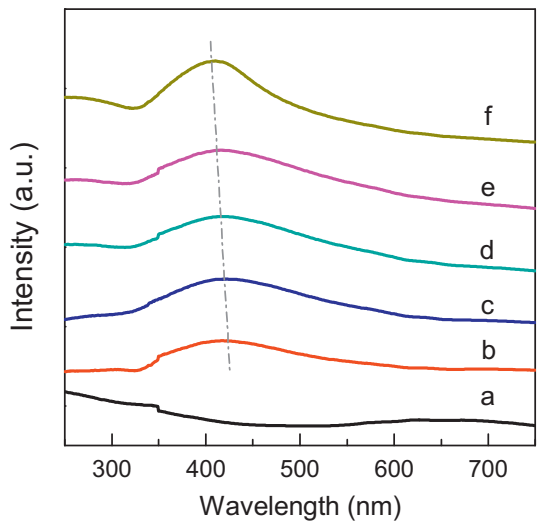

Fig. 5 – UV–Vis DRS of various catalysts. (a) 5Cu/SBA-15, (b) $5Ag_1$-$Cu_{0.4}$/SBA-15, (c) $5Ag_1$-$Cu_{0.2}$/SBA-15, (d) $5Ag_1$-$Cu_{0.1}$/SBA-15, (E) $5Ag_1$-$Cu_{0.05}$/SBA-15, and (f) 5Ag/SBA-15. UV–Vis DRS: ultraviolet–visible light diffuse reflectance spectra.

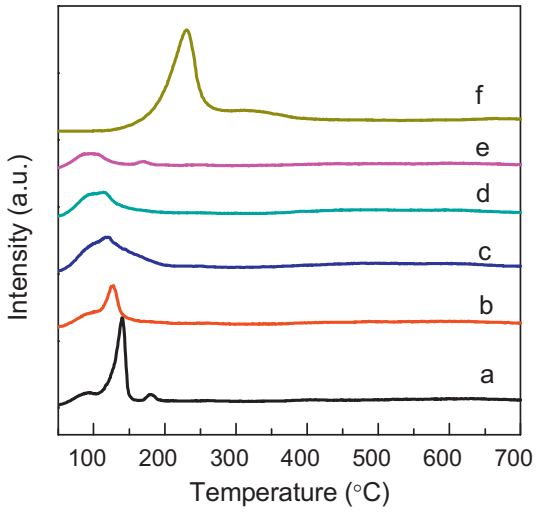

Fig. 6 – H_2–TPR profiles of the samples. (a) 5Ag/SBA-15, (b) $5Ag_1$-$Cu_{0.05}$/SBA-15, (c) $5Ag_1$-$Cu_{0.1}$/SBA-15, (d) $5Ag_1$-$Cu_{0.2}$/SBA-15, (e) $5Ag_1$-$Cu_{0.4}$/SBA-15, and (f) 5Cu/SBA-15.

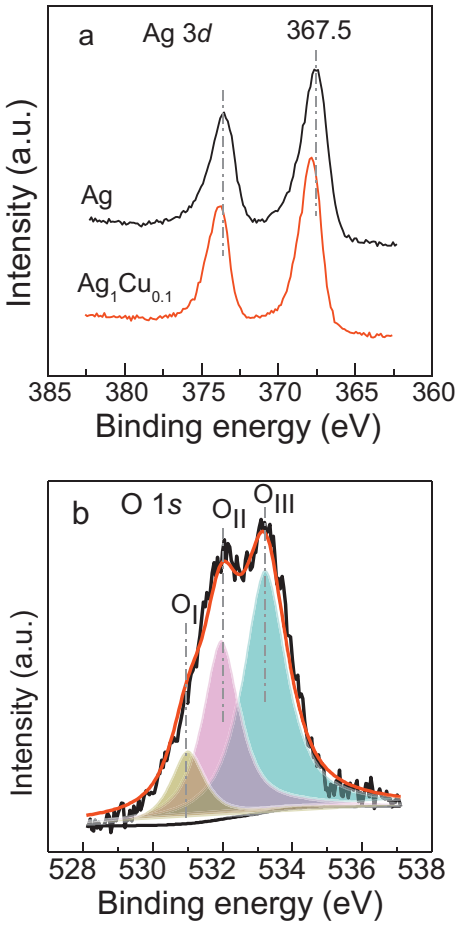

Fig. 7 – XPS spectrum of (a) Ag 3d and (b) O 1s on the surface of the $5Ag_1$-$Cu_{0.1}$/SBA-15 catalyst.

and dispersity of Ag NPs. Therefore, metal BE slightly shifts and moves to higher or lower values. In the bimetallic Ag–Cu sample, the state of the Ag species was positive ($Ag^{\delta+}$) likely due to the presence of the surrounding oxygen. As shown in Fig. 7, the Ag $3d_{5/2}$ peak of the bimetallic $5Ag_1$-$Cu_{0.1}$/SBA-15 catalysts gradually shifted to relatively higher BE values related to the monometallic Ag/SBA-15 catalyst. This result implied the occurrence of an interaction between Ag and Cu species (Wang et al., 2012b), as verified by UV–Vis and H_2–TPR.

In the process of diesel soot undergoing catalytic combustion, the active oxygen species induced by highly dispersed nanomaterials plays a vital role in its catalytic reactivity. The O 1s XPS profiles of $5Ag_1$-$Cu_{0.1}$/SBA-15 were obtained to clarify the oxygen species. As shown in Fig. 7b, the O 1s XPS peak of the sample $5Ag_1$-$Cu_{0.1}$/SBA-15 can be deconvoluted into three components at around 530.9, 531.9, and 533.2 eV after Gaussian fitting. These elements correspond to lattice oxygen O_I, hydroxyl oxygen O_{II}, and adsorbed oxygen O_{III}, respectively (Zhou et al., 2015a; Wang et al., 2012a). The $5Ag_1$-$Cu_{0.1}$/SBA-15 bimetallic catalyst possessed an abundant surface-adsorbed oxygen species as high as 53.2% (Table 2). This phenomenon could be ascribed to the potential capability for O_2 activation on the Ag–Cu alloy NPs. The oxygen absorption and activation are likely related to the catalytic activity. In other words, their superior catalytic properties are believably related to the increased concentration of surface active oxygen species.

2.3. Thermodynamic analysis

Apparent activation energy is a valuable parameter in the discussion of soot combustion mechanism. In our study, activation energy values can be derived by processing the DTA data *via* Ozawa method on the basis of the plots of $\log\varphi$ *versus* $1/T$ for a soot combustion conversion of 50% (Fig. 8). In particular, the activation energies of $5Ag_1$-$Cu_{0.1}$/SBA-15, 5Ag/SBA-15, and 5Cu/SBA-15 were evaluated at 50% soot conversion (Fig. 9). The activation energies of $5Ag_1$-$Cu_{0.1}$/SBA-15 obtained a much lower E_a value of 123.3 kJ/mol than 5Ag/SBA-15 (130.7 kJ/mol) and 5Cu/SBA-15 (145.6 kJ/mol). The results indicated that the production or activation of relevant oxygen species involving a reaction mechanism over bimetallic catalysts might be changed. Compared with a pure Cu catalyst, Ag activates oxygen molecules, but its practical applications are hindered by the affinity of Ag NPs to sintering. In contrast to monometallic 5Ag/SBA-15, with the catalytic performance and characterization of bimetallic Ag–Cu catalysts, the formed Ag–Cu nanoalloys provided not only the stable and dispersed NPs but also the abundant surface-adsorbed oxygen species. As a result, the efficiency of catalytic combustion was greatly enhanced, compared with that of a monometallic catalyst.

Table 2 – Surface oxygen species of the catalyst $5Ag_1$-$Cu_{0.1}$/SBA-15 analyzed by XPS.

Element	O_I	O_{II}	O_{III}
Binding energy (eV)	530.9	531.9	533.2
Percentage of total area (%)	12.8	34.0	53.2

XPS: X-ray photoelectron spectroscopy.

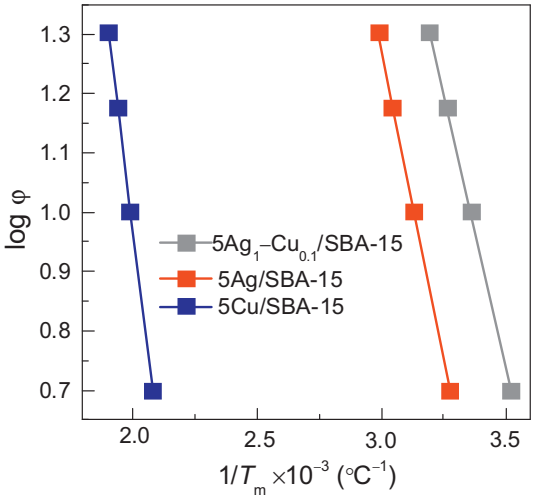

Fig. 8 – Plots of Ozawa for the determination of the activation energy of soot combustion on 5Ag/SBA-15, 5Cu/SBA-15, and $5Ag_1$-$Cu_{0.1}$/SBA-15 catalysts.

3. Conclusions

The bimetallic Ag–Cu/SBA-15 catalysts were prepared by co-impregnation method. The addition of Cu into Ag helped dispersing the Ag–Cu bimetallic NPs by forming Ag–Cu alloys. The bimetallic Ag–Cu/SBA-15 catalysts afforded enhanced catalytic performance and stability for the complete soot combustion. The optimized Ag/Cu atomic ratio was approximately 1:0.1, with which the catalyst ignited the soot combustion at T_{ig} = 225°C with a T_{50} = 285°C and exhibited negligible decay in the complete soot combustion for five cycles. A synergistic effect between Ag and Cu was proposed to explain the observation. The alloying of Ag and Cu electronically modified the Ag and Cu domains, shifting the Ag_{3d} core-levels and promoting charge transfer between Cu and Ag in a manner that favored for O_2 adsorption and activation. The increment in surface active oxygen concentration was believed to be making contributions to the superior catalytic activity. We envisioned that the proposed bimetallic Ag–Cu NPs catalysts with higher density of active oxygen species can be applied to other processes involving oxygen activation and active oxygen transformation, such as CO selective oxidation and water-gas shift reaction.

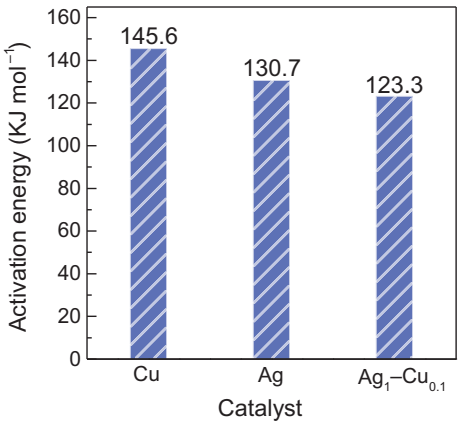

Fig. 9 – Activation energy of 50% soot combustion on the catalysts: $5Ag_1$-$Cu_{0.1}$/SBA-15, 5Ag/SBA-15, and 5Cu/SBA-15.

Acknowledgments

We gratefully acknowledge the National Natural Science Foundation of China (Nos. 21403178, 21473145, 21503173, and 91545115), the National High-tech R&D Program (2015AA03A402), and the Program for Innovative Research Team in Chinese Universities (No. IRT_14R31).

Appendix A. Supplementary data

Supplementary data to this article can be found online at http://dx.doi.org/10.1016/j.jes.2016.12.021.

REFERENCES

Aneggi, E., Leitenburg, C.D., Dolcetti, G., Trovarelli, A., 2008. Diesel soot combustion activity of ceria promoted with alkali metals. Catal. Today 136, 3–10.

Aneggi, E., Llorca, J., Leitenburg, C.D., Dolcetti, G., Trovarelli, A., 2009. Soot combustion over silver-supported catalysts. Appl. Catal. B Environ. 91, 489–498.

Bueno-López, A., 2014. Diesel soot combustion ceria catalysts. Appl. Catal. B Environ. 146, 1–11.

Cao, A., Veser, G., 2009. Exceptional high-temperature stability through distillation-like self-stabilization in bimetallic nanoparticles. Nat. Mater. 9, 75–81.

Chen, L.F., Guo, P.J., Qiao, M.H., Yan, S.R., Li, H.X., et al., 2008. Cu/SiO_2 catalysts prepared by the ammonia-evaporation method: texture, structure, and catalytic performance in hydrogenation of dimethyl oxalate to ethylene glycol. J. Catal. 257, 172–180.

Corro, G., Pal, U., Ayala, E., 2013. Diesel soot oxidation over silver-loaded SiO_2 catalysts. Catal. Today 212, 63–69.

Creighton, J.A., Eadon, D.G., 1991. Ultraviolet–visible absorption spectra of the colloidal metallic elements. J. Chem. Soc. Faraday Trans. 87 (24), 3881–3891.

Czaplinska, J., Sobczak, I., Ziolek, M., 2014. Bimetallic AgCu/SBA-15 system: the effect of metal loading and treatment of catalyst on surface properties. J. Phys. Chem. C 118, 12796–12810.

Huang, Y., Ariga, H., Zheng, X.L., Duan, X.P., Takakusagi, S., Yuan, Y.Z., et al., 2013. Silver-modulated SiO_2-supported copper catalysts for selective hydrogenation of dimethyl oxalate to ethylene glycol. J. Catal. 307, 74–83.

Kayama, T., Yamazaki, K., Shinjoh, H., 2010. Nanostructured ceria-silver synthesized in a one-pot redox reaction catalyzes carbon oxidation. J. Am. Chem. Soc. 132, 13154–13155.

Liang, Q., Wu, X.D., Weng, D., 2008. Oxygen activation on Cu/Mn–Ce mixed oxides and the role in diesel soot oxidation. Catal. Today 139, 113–118.

Liu, X.Y., Wang, A.Q., Wang, X., Mou, C.Y., Zhang, T., 2008. Au–Cu alloy nanoparticles confined in SBA-15 as a highly efficient catalyst for CO oxidation. Chem. Commun. 3187-3189.

Ozawa, T., 1965. A new method of analyzing thermogravimetric data. Chem. Soc. Jpn. 38, 1881–1886.

Serra, V., Saracco, G., Badini, C., 1997. Combustion of carbonaceous materials by Cu–K–V based catalysts II. Reaction mechanism. Appl. Catal. B Environ. 11, 329–346.

Sudarsanam, P., Hillary, B., Deepa, D.K., Amin, M.H., Mallesham, B., Bhargava, S.K., et al., 2015. Highly efficient cerium dioxide nanocube-based catalysts for low temperature diesel soot oxidation: the cooperative effect of cerium- and cobalt-oxides. Catal. Sci. Technol. 5, 3496–3500.

Twigg, Martyn V., 2007. Progress and future challenges in controlling automotive exhaust gas emissions. Appl. Catal. B Environ. 70, 2–15.

Uchisawa, J.O., Obuchi, A., Zhao, Z., Kushiyama, S., 1998. Carbon oxidation with platinum supported catalysts. Appl. Catal. B Environ. 18, L183–L187.

Ura, B., Trawczynski, J., Lopez-Suarez, F.E., Bieniasz, W., Ilan-Gomez, M.J., Bueno-lopez, A., et al., 2011. Effect of potassium addition on catalytic activity of $SrTiO_3$ catalyst for diesel soot combustion. Appl. Catal. B Environ. 101, 169–175.

Wang, X., Jiang, Z.Y., Xie, Z.X., Zheng, L.S., 2012a. Synthesis and shape-dependent catalytic properties of CeO_2 nanocubes and truncated octahedral. CrystEngComm 14, 7579–7582.

Wang, Y.N., Duan, X.P., Zheng, J.W., Lin, H.Q., Yuan, Y.Z., Ariga, H., et al., 2012b. Remarkable enhancement of Cu catalyst activity in hydrogenation of dimethyl oxalate to ethylene glycol using gold. Catal. Sci. Technol. 2, 1637–1639.

Wei, Y.C., Liu, J., Zhao, Z., Duan, A.J., Jiang, G.Y., Xu, C.M., et al., 2011. Three-dimensionally ordered macroporous $Ce_{0.8}Zr_{0.2}O_2$-supported gold nanoparticles: synthesis with controllable size and super-catalytic performance for soot oxidation. Energy Environ. Sci. 4, 2959–2970.

Wei, Y.C., Zhao, Z., Jin, B.F., Yu, X.H., Jiao, J.Q., Li, K.X., et al., 2014. Synthesis of AuPt alloy nanoparticles supported on 3D ordered macroporous oxide with enhanced catalytic performance for soot combustion. Catal. Today 251, 103–113.

Xu, J.F., Liu, J., Zhao, Z., Xu, C.M., Zheng, J.X., Duan, A.J., et al., 2011. Easy synthesis of three-dimensionally ordered macroporous $La_{1-x}K_xCoO_3$ catalysts and their high activities for the catalytic combustion of soot. J. Catal. 282, 1–12.

Zhao, D.Y., Huo, Q.S., Feng, J.L., Chemlka, B.F., Stucky, G.D., 1998. Nonionic triblock and star diblock copolymer and oligomeric surfactant syntheses of highly ordered, hydrothermally stable, mesoporous silica structures. J. Am. Chem. Soc. 120, 6024–6036.

Zheng, J.W., Lin, H.Q., Wang, Y.N., Zheng, X.L., Duan, X.P., Yuan, Y.Z., 2013. Efficient low-temperature selective hydrogenation of esters on bimetallic Au-Ag/SBA-15 catalyst. J. Catal. 297, 110–118.

Zhou, Z.M., Pang, S.P., Liu, Z.H., Xu, H.X., Cui, G.L., 2015a. Interface engineering for high-performance perovskite hybrid solar cells. J. Mater. Chem. A 3, 19205–19217.

Zhou, J.F., Duan, X.P., Ye, L.M., Zheng, J.W., Li, M.M.J., Yuan, Y.Z., et al., 2015b. Enhanced chemoselective hydrogenation of dimethyl oxalate to methyl glycolate over bimetallic Ag-Ni/SBA-15 catalysts. Appl. Catal. A Gen. 505, 344–353.